TITLE: Artificial Sputum Medium Formulation Impacts *Pseudomonas aeruginosa* Phenotype and Chemotype

AUTHORS: Rachel L. Neve[1] and Vanessa V. Phelan[2#]

AUTHOR AFFILIATIONS:

[1] Department of Immunology and Microbiology, School of Medicine, University of Colorado - Anschutz Medical Campus, Department of Immunology and Microbiology, Aurora, CO, 80045, USA

[2] Department of Pharmaceutical Sciences, Skaggs School of Pharmacy and Pharmaceutical Sciences, University of Colorado - Anschutz Medical Campus, Aurora, CO, 80045, USA

CORRESPONDING AUTHOR:

[#] Address correspondence to Vanessa V. Phelan, vanessa.phelan@cuanschutz.edu

ABSTRACT

Artificial sputum medium (ASM) is a class of *in vitro* bacterial culture medium intended to mimic the nutritional environment of cystic fibrosis (CF) pulmonary mucus. One of the most commonly studied microbes in ASM is *Pseudomonas aeruginosa,* a prevalent and dangerous pathogen of the CF pulmonary microbiome. Many ASM formulations have been reported in literature, with differing nutrient concentrations and availability. Here, we show that common formulations of ASM yield different phenotypes and chemotypes of *P. aeruginosa*. Further, we demonstrate that iron in commercial porcine gastric mucin (PGM) is sufficient to alter production of *P. aeruginosa* siderophores in the chemically defined ASM, synthetic CF medium 1 (SCFM1). These results highlight that the choice of ASM formulation for *in vitro* investigations of microbial pathogenicity, physiology, and interactions should be carefully considered.

IMPORTANCE

In vitro culture media are being developed to resemble the *in vivo* nutritional environment more closely. These culture media are used to investigate microbial pathogenicity and ecology in environments that are more reflective of disease states. In cystic fibrosis (CF), a number of different artificial sputum media (ASM) formulations have been created to recapitulate the CF lung environment. However, these ASM have different sources and concentrations of nutrients. Here, we cultured *Pseudomonas aeruginosa* in nine different formulations of ASM. *P. aeruginosa* is the primary pathogen causing lung infection in CF.

We show that different ASM formulations lead to different phenotypes and chemotypes by *P. aeruginosa* and one component of ASM, mucin, contains high levels of iron, which may affect *P. aeruginosa* physiology.

Cystic fibrosis (CF) is a genetic disease characterized by the accumulation of thick bronchial mucus, which causes decreased mucociliary clearance and enables the growth of pathogenic bacteria and fungi. Pulmonary mucus is a nutritionally distinct environmental niche comprised of mucin, DNA, amino acids, lipids, and micronutrients, including metals (1, 2). To study the physiology of microbial pathogens and communities in the unique CF pulmonary environment, a variety of artificial sputum media (ASM) have been developed (3-14), and applied to investigate microbial physiology (3, 5, 15-17), biofilm morphology (10, 18), antibiotic susceptibility (19, 20), and interspecies interactions in the context of CF (21-23). However, disparate nutrient concentration and bioavailability between ASM formulations may affect microbial growth, metabolism, and virulence (3, 7, 20, 24).

Pseudomonas aeruginosa is one of the most common opportunistic pathogens affecting CF patients, with colonization starting in childhood and affecting more than half of adults (25). Chronic *P. aeruginosa* pulmonary infections cause progressive loss of lung function (26), leading to premature death (25). Due to its importance, *P. aeruginosa* is well-studied in terms of its genome plasticity (27), biofilm growth (28), adaptations (29), development of antibiotic resistance (27, 29-31), and production of virulence factors in the CF lung (32-34). While *P. aeruginosa* produces a vast array of virulence factors, key components of the interactions between *P. aeruginosa* and the environment are its specialized metabolites (3, 4, 6-8, 10, 11), including phenazines (PHZs), quinolones (AQs), rhamnolipids (RHLs), and siderophores. These specialized metabolites function as quorum sensing signals (35), electron shuttles (36), biosurfactants (37), iron scavenging molecules (35, 38-40), and antimicrobials (40-42).

Herein, we investigated the effect of nine ASM formulations on *P. aeruginosa* PAO1 phenotype and specialized metabolite chemotype. We observed that the phenotype of PAO1 was greatly altered in disparate ASM formulations. Using molecular networking (MN) (43, 44) guided analysis of non-targeted metabolomics data, we determined that all ASM formulations induced the production of a similar suite of specialized metabolites. However, production of individual specialized metabolites and summed total of molecular families were statistically different between ASM formulations. Our results show that PAO1 cultured in ASM formulations with different nutrient concentration and bioavailability yield different *P. aeruginosa* specialized metabolism. Further, we show that commercial porcine gastric mucin (PGM), a component of most ASM formulations, is as an unexpected source of iron, which alters *P. aeruginosa* siderophore production and implicates the inclusion of complex biomolecules in otherwise chemically defined media as sources of other nutrients.

RESULTS AND DISCUSSION

ASM formulation affects *Pseudomonas aeruginosa* phenotype. *In vitro* cultivation of microbial pathogens has enabled thorough investigation of microbial physiology, gene expression, and virulence factor production. However, most of these investigations have been performed in standard laboratory media, which may not reflect the *in vivo* nutritional environment in which pathogens exist. In cystic fibrosis (CF), an effort to replicate the *in vivo* nutritional environment of the lung has resulted in the creation of a wide variety of *in vitro* culture media, broadly referred to as artificial sputum media (ASM). Most ASM formulations contain the major components of CF sputum, including mucin, DNA, amino acids, and a lipid source (45). However, the exact composition of

ASM varies between formulations with alterations based upon nutritional measurements from CF sputum, cited literature, personal observation, or cost of materials.

We hypothesized that culturing *P. aeruginosa* PAO1 in different ASM formulations would yield phenotypes. To test this hypothesis, PAO1 was cultured in nine commonly used ASM (3-8, 10, 11) (**Fig. 1 Timeline and composition alterations of common ASM formulations, Dataset S1 ASM Formulations**). These ASM formulations can be broken down into two lineages, complex and defined; both of which have contain the major components of CF sputum (45). The complex ASM lineage is derived from Soothill ASM (4). As Soothill ASM did not contain amino acids, Sriramulu *et al.* complemented the medium with 250 mg/L of each canonical amino acid to generate Romling ASM (9, 10). Winstanley ASM is compositionally identical to Romling, except for its buffering capacity (6). ASMDM ASM (3) is modified from Romling ASM by the addition of bovine serum albumin (BSA), and alterations in mucin and DNA concentration. Derived from ASMDM ASM, Cordwell ASM (5) has reduced buffering capacity, replacement of individual amino acids with casamino acids (Cas AA), and replacement of DTPA with ferritin to replicate CF sputum iron availability more accurately. SDSU ASM (8) is modified from Cordwell ASM by replacement of Cas AA with MEM amino acids (MEM AA), removal of BSA, and increasing the mucin concentration.

Recently, chemically defined Synthetic Cystic Fibrosis Medium (SCFM1) was developed from the average concentrations of ions, free amino acids, glucose, and lactate as measured from CF sputum samples (7). SCFM1 was supplemented with DNA, bovine submaxillary mucin (BSM), *N*-acetyl glucosamine (GlcNAc), and

dioleoylphosphatidylcholine (DOPC) at concentrations similar to those observed in CF sputum to create SCFM2 (11). SCFM2 was further modified by the addition of *p*-aminobenzoic acid (PABA), nicotinamide adenine dinucleotide (NAD^+), adenine (ADE), guanine (GUA), xanthine (XAN), and hypoxanthine (HX) to generate SCFM3, as experimental results suggested that these metabolites are more available in CF sputum than in SCFM2 (11). We used PGM was used as the mucin source as it is a cost effective and common replacement of BSM (12-14).

PAO1 grew in all media (**Fig. S1 Growth of PAO1 in ASM**); however, both the gross morphology and culture color varied between ASM formulations (**Fig. 2A PAO1 phenotype and metabolome in ASM and LB**). In Soothill ASM, the cultures were turbid, but, unlike the other ASM formulations, no macrostructures were visible. The Romling and Winstanley formulations both induced a brown macrostructure phenotype. In ASMDM ASM, *P. aeruginosa* grew heterogeneously with a layer of growth at the air-liquid interface, giving way to turbid growth further down the culture. In SDSU ASM, PAO1 formed a green, floating structure near the center of the well that reached the surface of the medium. PAO1 grew as a turbid culture with bright green coloration in SCFM1; while in SCFM2 and SCFM3, PAO1 growth was more structured with a distinctly blue color.

***P. aeruginosa* produces similar specialized metabolites in all ASM formulations.** As metabolism often underlies phenotypic changes, we hypothesized that different ASM formulations induced different chemotypes of PAO1. *P. aeruginosa* has a well characterized specialized metabolome chemical signals produced by microorganisms to interact with their environment (46, 47)), including six molecular families: homoserine

lactones (HSLs), rhamnolipids (RHLs), alkyl quinolones (AQs), phenazines (PHZs), and the siderophores pyochelin (PCH) and pyoverdine (PVD) (48-50). These compounds are chemically and functionally diverse and include quorum sensors, small molecule virulence factors, and natural products. *P. aeruginosa* specialized metabolites have been detected in CF sputum (32-34) and associated with pathogenicity and virulence (24, 50, 51).

To determine if different ASM formulations induced the production of different molecular families by *P. aeruginosa*, we analyzed non-targeted liquid chromatography tandem mass spectrometry (LC-MS/MS) data of PAO1 grown in ASM and LB using the classical molecular networking (CMN) workflow of the GNPS platform. Briefly, CMN organizes metabolites into molecular families using MS/MS spectral similarity as a proxy for structural similarity (43). CMN is best used for applications assessing the presence or absence of a molecular signal in an experiment (43, 52, 53). Of the 1,824 nodes in the network, 220 (12%) had spectral matches to the GNPS libraries, representing 120 unique compounds. These compounds included members of the PHZ, AQ, RHL molecular families as well as PCH (**Fig. 2B PAO1 phenotype and metabolome in ASM and LB**).

Closer examination of the CMN results revealed the presence of duplicate nodes representing the same compound. Therefore, to generate a more accurate assessment of unique MS1 mass-to-charge (*m/z)* values shared between cultures of PAO1, nodes with the same precursor *m/z* value were combined and a binary presence/absence table was created. Of 1,165 unique *m/z* values, 140 were present in all cultures (**Fig. 2C PAO1 phenotype and metabolome in ASM and LB**), including values corresponding

to the PHZ, AQ, and RHL molecular families, suggesting that all ASM formulations have the nutritional resources for PAO1 to produce these compounds. In addition to *m/z* values shared between all cultures of PAO1, a number of *m/z* values were detected in samples of PAO1 grown in specific media. PAO1 cultures in Soothill ASM had the most *m/z* values unique to a single medium (**Fig. 2D PAO1 phenotype and metabolome in ASM and LB**). GNPS library matches of these Soothill ASM associated *m/z* values largely represent fragmentation of media components, likely due to relative higher intensity of these peaks compared to other ASM formulations. The production levels of PAO1 metabolites of Soothill ASM cultures did not require dilution to prevent saturation of the MS detector.

ASM formulation alters the production levels of *P. aeruginosa* specialized metabolites. As PAO1 specialized metabolite presence was generally conserved across all ASM formulations, we applied the feature based molecular networking (FBMN) to quantify and visualize metabolite production levels of PAO1 in the different ASM formulations. FBMN integrates feature finding, a data reduction step in LC-MS analysis, with MN (44). Feature finding generates a quantitative representation of all metabolites within a metabolomics dataset by defining a feature as an *m/z*, retention time (RT), and corresponding abundance. In FBMN, LC-MS/MS data is processed feature finding to generate abundance from MS1 data, and one representative MS/MS spectrum is generated for each feature (*m/z*-RT pair). Like in CMN, MS/MS spectra from an experiment are organized into molecular families. However, in FBMN, abundance data is imported into the molecular network as pie charts to provide rapid visualization of differential abundance between metadata categories, such as ASM

formulation. Of the 492 nodes in the network, 80 (16%) had matches to GNPS library spectra, representing 60 unique compounds. Statistical analysis of the feature table revealed that the abundance of only two features were not statistically different between PAO1 cultures in ASM formulations (**Dataset S2 Statistics of ASM Metabolism Results**). *P. aeruginosa* production of individual and total PHZs, AQs, RHLs, PCH, and PVDs, were all altered in different ASM formulations. Notably, HSLs were not detected under our conditions.

PHZs are redox active virulence factors with various biological activities, including promoting iron uptake (36, 40), anaerobic respiration (36), biofilm formation (54, 55), and interspecies interactions (40, 48, 56, 57), among others (58-60). We quantified four PHZs: 1-hydroxyphenazine (1-HP), pyocyanin (PYO), phenazine-1-carboxamide (PCN), and phenazine-1-carboxylic acid (PCA) (**Fig. 3A Phenazines**). While PHZs were detected in all PAO1 cultures, total PHZ production by PAO1 varied between formulations with lowest production in Soothill ASM and highest production in SCFM2 and SCFM3 (**Fig. 3B Phenazines**). The low levels of PHZs produced by PAO1 in Soothill ASM is likely due to the absence of amino acids in the medium. In addition to variations in total PHZ production, the production of individual PHZs varied. In Soothill ASM, PAO1 produced primarily PCA. PCA has been implicated in inducing *P. aeruginosa* biofilm formation by enabling the reduction of Fe(III) to Fe(II) in a *P. aeruginosa* mutant unable to produce the siderophores PVD and PCH (61). As Soothill ASM is amino acid limited and restricts the precursor availability for siderophore biosynthesis by *P. aeruginosa* (62-64), PCA may be produced to acquire iron from the medium. *P. aeruginosa* produces higher levels of 1-HP in the Romling, Winstanley,

ASMDM, Cordwell, and SDSU ASM formulations. PYO is produced highest in SCFM2 and SCFM3, which contributes to the characteristic blue phenotype of these cultures. Interestingly, despite similar production ratios of PHZs in the SCFM series of ASM (**Fig. 3C Phenazines**), the total PHZ production by PAO1 in SCFM1 is significantly lower than in SCFM2 and SCFM3 (mean PHZ AUC SCFM1=3.28×10^4, SCFM2=1.38×10^5, SCFM3=1.34×10^5, $p<0.0001$). SCFM2 and SCFM3 (11) are compositionally different from SCFM1 by the addition of several components, including GlcNAc. An increase of PYO production by *P. aeruginosa* was measured spectrographically upon addition of GlcNAc (65). GlcNAc likely induces PYO production through a mechanism to sense and respond to peptidoglycan.

Like PHZ production, *P. aeruginosa* production of individual and total AQs varied depending upon ASM formulation. We quantified forty-three AQs from the PAO1 ASM cultures and only one could not be annotated (**Fig. 4A Quinolones**). Total AQ production by *P. aeruginosa* was highest in Romling, Winstanley, and ASMDM ASM formulations, all at similar levels (mean = ~4×10^5), and lowest in Soothill and SDSU ASM (**Fig. 4B Quinolones**). Different AQs have different roles in intra- and interspecies interactions within the CF lung environment (66-70). 2-heptyl-4-hydroxyquinolone-N-oxide (HQNO) is a potent inhibitor of the respiratory chain of microbial and host cells (66, 67). 2-heptyl-4-hydroxyquinolone (HHQ) is an autoinducer of the *pqs* operon (68), and 2-heptyl-3,4-dihydroxyquinolone (Pseudomonas Quinolone Signal, PQS) potentiates HSL-dependent QS (69), biofilm formation (70), and siderophore production (68). AQs were classified as HHQ-type, PQS-type, or HQNO-type based on their MS/MS fragmentation patterns (56, 71). AQ production by PAO1 in all ASM

formulations was predominantly HHQ-type AQs (~44-76%), while HQNO-type AQs accounted for ~15-41%, and PQS-type AQs were the consistently the least abundant (~3-17%) (**Fig. 4C Quinolones**).

RHLs have functional roles in biofilm formation and maintenance (72, 73), motility as biosurfactants (37), competition with fungal neighbors (41), and evasion of the host immune response (74, 75). Six RHLs were quantified (**Fig. 5A Rhamnolipids**). Total PAO1 RHL production was lower in Romling, SCFM2, and SCFM3 (means = $2.9x10^4$, $1.8x10^4$, $2.2x10^4$, respectively) ASM formulations compared to the other versions of ASM (range of means = $3.6x10^4$ - $4.0x10^4$) (**Fig. 5B Rhamnolipids**). The proportion of mono- to di-RHL production was maintained across cultures in all ASM, with 30.0 - 43.8% mono-RHLs. The predominant fatty acid length was C10, accounting for 56.2 - 70.0% of RHLs produced (**Fig. 5C Rhamnolipids**). The production of RHLs is dependent on the *rhl* QS system; specifically the binding of the autoinducer C4-HSL, produced by RhlI, to the transcription factor RhlR (76). The RhlI/RhlR QS system is activated by the LasI/R QS system and directs the regulation of many virulence encoding genes (77, 78). Lower production levels of RHLs by PAO1 may indicate altered QS signaling, which may affect the production of other virulence factors.

Strikingly, production of siderophores by *P. aeruginosa* was almost exclusive to SCFM1 cultures (**Fig. 6 Siderophores**). Siderophores are metal scavenging virulence factors (79, 80), secreted in low iron conditions to compete for environmental iron (81). *P. aeruginosa* produces two siderophores, PVD and PCH (38), with PVD having a higher affinity for iron than PCH (38). While PCH was identified in SCFM1 cultures based upon a match to GNPS libraries, the nodes corresponding to the PVD molecular

family were prioritized for annotation based upon coloration of the pie chart, which indicated high production by PAO1 in SCFM1 (**Fig. 6A Siderophores**). Although PVD biosynthesis was reported to be upregulated in SCFM1 (7), we were surprised to detect PVDs as the production of this molecular family by PAO1 is below our limit of detection when cultured in most media. The rapid visualization of molecular families and their production levels in FBMN enabled us to identify this molecular family in a non-biased manner, when we were admittedly not expecting to observe its production.

Addition of commercial PGM to SCFM1 reduces PAO1 siderophore production due to the presence of iron. As the production of PCH and PVD is triggered by low environmental iron (82), the production of PCH and PVD by *P. aeruginosa* in SCFM1 was surprising as all ASM formulations contain similar concentrations of added iron. Soothill ASM was measured to have 9.5 µM Fe^{2+} prior to addition of DTPA (15 µM) as an iron chelator (4). Both Cordwell and SDSU ASM contain 0.000003% (w/v) ferritin, which adds ~2.85 µM Fe^{2+} to the media. Furthermore, SCFM1, SCFM2, and SCFM3 formulations contain 3.60 µM Fe^{2+}. Taken together, the inability to detect siderophores after PAO1 growth in all ASM except SCFM1 suggests these formulations contain an undefined source of iron.

To replicate the CF lung environment more closely, SCFM1 was modified by the addition of DNA, DOPC, GlcNAc, and mucin to create SCFM2 (11). As PGM was the most complex additive to our SCFM2 formulation, we hypothesized that commercial PGM was a source of contaminating iron in ASM. Mucins are a critical component of *in vitro* culture media for modeling the microbial interactions of CF lung infections (13, 83, 84), as well as other mucosal body sites (85, 86). The mucin concentration of CF

sputum ranges from 16-30 mg/mL (1). In the lung, mucin is a source of nutrients for inhabiting microbes (2, 87, 88) and also is involved in microbial adhesion (87), aggregation (89, 90) and dispersion (83).

To test if the addition of PGM to SCFM1 altered siderophore production by *P. aeruginosa*, PAO1 was cultured in SCFM1 and SCFM1 complemented with 0.5% (w/v) PGM (**Fig. S2 Growth of PAO1 in SCFM1 and SCFM1 with PGM**). Quantification of PCH and PVD molecular families revealed that the addition of PGM to SCFM1 was sufficient to reduce siderophore production by *P. aeruginosa* (**Fig. 7A, 7B PGM iron content and impact on PAO1 siderophores**). As measured by ICP-MS, 0.5% (w/v) of PGM contains 30.6 μM iron, which is 8.5 times higher than the concentration of iron added to the SCFM1 base medium (3.6 μM) (**Fig. 7C PGM iron content and impact on PAO1 siderophores**). Due to increased PGM concentration, ASMDM and Cordwell ASM contain ~60 μM iron and SDSU ASM contains ~117 μM.

Importance of ASM formulation on *in vitro* investigations. The differential production of specialized metabolites by PAO1 grown in different ASM has important implications for the interpretation of experimental results performed in this class of media. It is well established that *P. aeruginosa* specialized metabolites play important roles in virulence (36, 38), microbial interactions (40-42), and nutrient acquisition from the environment (35, 38-40). While the conclusions from a single dataset are valid, comparing the results between experiments performed in different ASM formulations should be carefully considered. For example, PYO is produced in highest abundance by PAO1 in SCFM2 and SCFM3. PYO is known to affect respiratory epithelial functions, including cellular respiration, electron transport, and innate immune response

mechanisms (60, 91-94). If the culture supernatants of PAO1 in SCFM2 and SDSU ASM were used to investigate the effect of PAO1 exometabolome on lung epithelial cells, the results of those experiments would likely vary significantly due to the differential production of PYO.

Similarly, many of the *P. aeruginosa* specialized metabolites are important in interspecies microbial interactions. The PHZ 1-HP is important in interactions between *P. aeruginosa* and the fungal pathogen *Aspergillus fumigatus* (40, 95). Treating *A. fumigatus* cultures with supernatants from PAO1 grown in Romling ASM and SCFM2 would likely lead to different results. The *P. aeruginosa* AQ HQNO is known to alter *S. aureus* susceptibility to antibiotics (96). Therefore, differential production of HQNO by *P. aeruginosa* in different ASM could affect the results of antibiotic susceptibility assays performed in different ASM formulations.

Last, siderophores are important for iron competition *in vivo* and loss of siderophore production affects the production of other specialized metabolite molecular families by *P. aeruginosa* (97). Inclusion of PGM in SCFM1 increases the concentration of iron in the medium to a more clinically relevant level of iron (98-100), leading to decreased production of PCH and PVD. However, the distinct iron sources in PGM are unknown and may not represent those in the CF lung (99, 101). If investigators desire to test iron concentration or source on *P. aeruginosa* and other microbes, PGM inclusion and concentration in the medium may influence the outcome of their experiments.

CONCLUSION

In vitro model systems are attractive due to their broad accessibility and ability to probe hypotheses thoroughly. The foundation of an *in vitro* investigation is the medium. In CF,

a broad suite of different ASM formulations has been created. In this study, we demonstrated that differences in nutritional content between ASM formulations alter the phenotype and chemotype of *P. aeruginosa* PAO1. Importantly, the concentration of specialized metabolites, including members of the AQ, PHZ, RHL, and siderophore molecular families, are impacted by ASM formulation. Given the role of these metabolites in virulence, differences in ASM formulation may influence the overall outcome of interactions among *P. aeruginosa*, the host, and other members of the CF pulmonary microbiota. Commercial PGM was identified as a source of contaminating bioavailable iron, influencing siderophore production by *P. aeruginosa*. In view of the importance of mucin in replicating mucosal infection environments *in vitro,* further work is needed to understand the contribution of commercial mucin to bioavailable nutrients in culture media more fully. Therefore, careful consideration should be used when comparing results across studies employing different ASM formulations.

MATERIALS AND METHODS

General: *Pseudomonas aeruginosa* PAO1 (MPAO1) was acquired from the University of Washington, Seattle (102). All media components, concentrations, and commercial sources for artificial sputum media (ASM) formulations are listed in **Dataset S1 ASM formulations** (3-11). Miller Luria broth (LB) and porcine gastric mucin type III (PGM) were purchased for Millipore Sigma. Organic solvents for extraction and liquid chromatography tandem mass spectrometry (LC-MS/MS) analysis were purchased from VWR (ethyl acetate (EtOAc), HiPerSolv Chromanorm purity) and Fisher Scientific (methanol (MeOH), acetonitrile (ACN), formic acid (FA), and water; all Optima LC/MS grade). PA Mix was created as a set of external standards for *P. aeruginosa* specialized

metabolite annotation. PA Mix contains 10 µM of each of the following: 1-hydroxyphenazine (1-HP, Tokyo Chemical Industry); pyocyanin (PYO, Sigma); phenazine-1-carboxylic acid (PCA, Ark Pharm); phenazine-1-carboxamide (PCN, Ark Pharm); 2-heptylquinolin-4(1H)-one (HHQ, Ark Pharm); 2-heptyl-4-hydroxyquinoline *N*-oxide (HQNO, Cayman Chemical); 2-heptyl-3-hydroxyl-4-quinolone (Pseudomonas Quinolone Signal, PQS, Chemodex); N-butyryl-l-homoserine lactone (C4-HSL, Cayman Chemical); N-(3-oxododecanoyl)-l-homoserine lactone (3-oxo-C12-HSL, Millipore Sigma); and a rhamnolipid mixture (RHL, AGAE Technologies, 90% pure).

Identification of commonly used ASM formulations: The Web of Science Core Collection (Clarivate Analytics) was searched for papers with the 'TOPIC' terms: "sputum medium", "sputum media", "cystic fibrosis medium", "cystic fibrosis media", "sputa media", "sputa medium", "CF media", or "CF medium" in the title, abstract, or keywords fields on May 10, 2020. All terms were searched as shown, including quotation marks. The results of this search were analyzed using the Web of Science tools 'Create Citation Report' and 'Analyze Results'. The Analyze Results tool was used to download data corresponding to Web of Science Categories. The citation report was used to select ASM formulations that were commonly cited.

Preparation of media: LB broth was prepared according to manufacturer instructions. Commercial PGM was suspended in 1X 3-morpholinopropane-1-sulfonic acid (MOPS) buffer (pH 7.0) to make a 10% (w/v) suspension, sterilized using a liquid autoclave cycle (<20 minute sterilization time), and an aliquot was checked for sterility before use. ASM formulations were prepared as reported (3-11) with the following modifications. Antibiotics were not included in any medium. For the Cordwell formulation (5), the

reported 0.1% (w/v) agar was excluded. For SCFM2 and SCFM3 (11), bovine submaxillary mucin (BSM) was replaced with PGM at the published concentration, a common substitution (12-14). Each ASM formulation was brought to the published pH (3-11). All media was stored in the dark at 4°C, checked for sterility prior to use, and used within one month of preparation.

Cultivation of *P. aeruginosa* in LB and ASM formulations: PAO1 was inoculated from a streak plate into 5 mL LB broth and incubated overnight at 37°C, shaking at 220 RPM. 1.98 mL of LB or ASM were inoculated with 20 µL of *P. aeruginosa* LB broth culture (OD_{600} of 0.05; ~10^6 CFU/mL final concentration) in polystyrene 24 well plates (6). For assessing *P. aeruginosa* growth and specialized metabolite production, each medium was evaluated in its own 24 well plate (12 medium control wells and 12 growth wells per medium). The media were inoculated and processed in three batches, comprised of 2-4 ASM formulations and a parallel LB plate as a control. All plates were covered and incubated statically at 37°C for 72 hours. For assessing the addition of PGM to SCFM1 on *P. aeruginosa* growth and specialized metabolite production, *P. aeruginosa* was cultured in SCFM1 and PGM-SCFM1 in a single polystyrene 24 well plate (4 medium control wells and 4 growth wells per medium).

Processing of *P. aeruginosa* cultures in LB and ASM formulations: Gross phenotypes of *P. aeruginosa* growth were photographed using a top-down view with a Stemi 508 stereo microscope with an Axiocam 105 color camera (Zeiss). Following visualization, 100 µL cellulase (*Aspergillus niger*, 100 mg/mL in sterile water; Sigma) was added to each well and aggregates were mechanically disrupted by pipetting using wide-bore pipette tips (USA Scientific), followed by water bath sonication (Branson) for

10 minutes, and a secondary mechanical disruption by pipetting using wide-bore pipette tips. Disrupted samples were aliquoted for measurements of growth (CFUs), pH, and metabolomics analysis. Three representative biological replicates from each culture condition were serially diluted, spotted onto LB agar, incubated at 37°C overnight, and counted to determine CFU/mL (**Fig. S1 Growth of PAO1 in ASM**).

Processing of *P. aeruginosa* cultures in SCFM1 and PGM-SCFM1: Gross phenotypes of *P. aeruginosa* growth were photographed using a top-down view with a Stemi 508 stereo microscope with an Axiocam 105 color camera (Zeiss). Following visualization, aggregates were mechanically disrupted by pipetting using wide-bore pipette tips (USA Scientific). Disrupted samples were aliquoted for measurements of growth (CFUs), pH, and metabolomics analysis. All four biological replicates from each culture condition were serially diluted, spotted onto LB agar, incubated at 37°C overnight, and counted to determine CFU/mL (**Fig. S2 Growth of PAO1 in SCFM1 with and without PGM**).

Sample preparation for LC-MS/MS: Each sample aliquot was chemically disrupted with an equal volume of 1:1 EtOAc:MeOH. The samples were dried, resuspended in 100% MeOH containing 1 µM glycocholic acid (Calbiochem, 100.1% pure), diluted as needed in 100% MeOH containing 1 µM glycocholic acid, and centrifuged for 10 min at 4,000 RPM (Thermo Sorvall ST 40R) to remove non-soluble particulates. Samples were diluted as follows for measurement of *P. aeruginosa* specialized metabolite production in ASM formulations and LB: not diluted: Soothill ASM; 5-fold dilution: Romling ASM, Cordwell ASM, SCFM1, SCFM2, and SCFM3; 10-fold dilution: Winstanley ASM,

ASMDM, SDSU ASM, and LB. All samples for measurement of *P. aeruginosa* specialized metabolite production in SCFM1 and SCFM + PGM were diluted 10-fold.

LC-MS/MS analysis: Mass spectrometry data acquisition for all samples was performed using a Bruker Daltonics Maxis II HD qTOF mass spectrometer equipped with a standard electrospray ionization (ESI) source. The mass spectrometer was tuned by infusion of Tuning Mix ESI-TOF (Agilent Technologies) at a 3 µL/min flow rate. For accurate mass measurements, a wick saturated with Hexakis(1H,1H,2H-difluoroethoxy) phosphazene ions (Apollo Scientific, *m/z* 622.1978) located within the source was used as a lock mass internal calibrant. Samples were introduced by an Agilent 1290 UPLC using a 10 µl injection volume. Extracts were separated using a Phenomenex Kinetex 2.6 µm C18 column (2.1 mm x 50 mm) using a 9 minute, linear water-ACN gradient (from 98:2 to 2:98% water:ACN) containing 0.1% FA at a flow rate of 0.5 mL/min. The mass spectrometer was operated in data dependent positive ion mode, automatically switching between full scan MS and MS/MS acquisitions. Full scan MS spectra (*m/z* 50 - 1500) were acquired in the TOF and the top five most intense ions in a particular scan were fragmented via collision induced dissociation (CID) using the stepping function in the collision cell. LC-MS/MS data for PA mix were acquired under identical conditions. Bruker Daltonics CompassXport was used to apply lock mass calibration and convert the LC-MS/MS data from .d format to .mzXML format.

Classical molecular networking (CMN) of *P. aeruginosa* specialized metabolism in LB and ASM formulations: A classical molecular network was created from the .mzXML files using the Molecular Networking workflow (version release 22) of the GNPS web platform (gnps.ucsd.edu,

https://gnps.ucsd.edu/ProteoSAFe/status.jsp?task=92a1c1f712904db4961fe0ff0dee3c2b) (43). Briefly, the data was filtered by removing all MS/MS fragment ions ± 17 Da of the precursor *m/z*. MS/MS spectra were window filtered by choosing only the top 6 fragment ions in each ± 50 Da window throughout the spectrum. The precursor ion mass tolerance was set to 0.1 Da and the MS/MS fragment ion tolerance to 0.2 Da. A network was then created where edges were filtered to have a cosine score above 0.7 and at least 5 matched fragment peaks between corresponding nodes. Further, edges between two nodes were kept in the network only if each of the nodes appeared in each other's respective top 10 most similar nodes. Finally, the maximum size of a molecular family was set to 100, and the lowest scoring edges were removed from molecular families until the molecular family was below this threshold. The spectra in the network were then searched against the GNPS spectral libraries. The library spectra were filtered in the same manner as the input data. All matches kept between the network spectra and library spectra were required to have a cosine score above 0.6 and at least 5 matched peaks. The molecular network was visualized using Cytoscape (version 3.7.1) (103).

Creation of UpSet plots from CMN results. The network table generated *via* CMN was downloaded from GNPS. As duplicate nodes representing the same metabolite were present in the network, precursor *m/z* values were rounded to the nearest hundredths and nodes with the same *m/z* values were combined to generate a list of unique *m/z* values. A binary presence/absence table was created to reflect whether MS/MS spectra corresponding to each *m/z* value was detected in each medium. The

binary table was visualized using the UpSetR Shiny App or in R using the UpSet package (104, 105).

Feature based molecular networking (FBMN) of *P. aeruginosa* specialized metabolism in LB and ASM formulations: MZmine (version 2.53) (106) was used to perform feature finding on the .mzXML files. The output was a feature table containing area under the curve (AUC) integration values for each feature (*m/z*-RT pair) and an .mgf file containing MS/MS spectra for each feature. The feature table was corrected for sample dilutions prior to submission to GNPS. A metadata table was created containing sample file names and attributes according to GNPS specifications. The Feature Networking workflow (version release 22) (44) was applied to the dilution-corrected feature table, .mgf file, and metadata file *via* the GNPS web platform (gnps.ucsd.edu, https://gnps.ucsd.edu/ProteoSAFe/status.jsp?task=baba5df5ab1b437980f81b4e64bcffc0) (43). Briefly, the data was filtered by removing all MS/MS fragment ions ± 17 Da of the precursor *m/z*. MS/MS spectra were window filtered by choosing only the top 6 fragment ions in each ± 50 Da window throughout the spectrum. The precursor ion mass tolerance was set to 0.05 Da and the MS/MS fragment ion tolerance was set to 0.1 Da. A network of nodes connected by edges was then created. Edges were filtered to have a cosine score above 0.75. Further, edges between two nodes were kept in the network only if each of the nodes appeared in each other's respective top 5 most similar nodes. Finally, the maximum size of a molecular family was set to 50, and the lowest scoring edges were removed from molecular families until the molecular family was below this threshold. The spectra in the network were then searched against the GNPS spectral libraries. The library spectra were filtered in the same manner as the input data.

All matches kept between the network spectra and library spectra were required to have a cosine score above 0.6 and at least 5 matched peaks. Sum normalization and mean aggregation were applied. The molecular network was visualized using Cytoscape (version 3.7.1) (103).

Feature annotation of *P. aeruginosa* specialized metabolites from FBMN results: All annotated features corresponding to *P. aeruginosa* specialized metabolites identified from FBMN analysis are listed in **Table S1. ASM metabolite annotation and mass defect**. Annotations of features corresponding to commercial standards (level 1 annotation (107)) were confirmed by comparing the experimental data (exact mass, MS/MS, and retention time) with data acquired for the compound in PA mix using Bruker Daltonics DataAnalysis v4.1 (Build 362.7). Putative annotation of specialized metabolites based on matches to the GNPS libraries (level 2 annotation (107)) and molecular families (level 3 annotation (107)) were validated by comparing the experimental data (exact mass, MS/MS) to reported data (56) and putative structures, respectively (56, 71) (**Fig. S3 Chromatograms of PVD family molecules from PAO1 in SCFM1**).

Metabolite, Molecular Family, and Sub-structure Class Annotation: Multiple features (different adducts, in-source fragments, and/or in-source dimers) can represent the same metabolite. Therefore, sum normalized AUC values for features corresponding to the same metabolite of interest (identified by co-elution and mass defect from predicted exact mass of the compound adduct, fragment, and/or dimer) were summed to provide the total AUC for a metabolite. Sum normalized AUC values for metabolites representing the same sub-structure class based upon MS/MS

fragmentation pattern (e.g. HHQ-type AQs or C10-C10 containing RHLs) were summed to provide the total AUC for a sub-structure class. Sum normalized AUC values for all identified metabolites representing the same molecular family based upon MS/MS fragmentation patterns (e.g. AQs or RHLs) were summed to provide the total AUC for a molecular family**.**

Targeted quantitation of *P. aeruginosa* siderophores in SCFM1 and PGM-SCFM1 cultures. MZmine (version 2.53) (106) was used to perform feature finding on the .mzXML files for *P. aeruginosa* growth in SCFM1 and PGM-SCFM1. Sum normalized AUC values for features corresponding to PCH, PVD, or their biosynthetic relatives (identified by co-elution and mass defect from predicted exact mass of the compound adduct, fragment, and/or dimer) were summed to provide the total AUC for each metabolite (**Table S2 SCFM1 and mucin siderophore annotation and mass defect**). Sum normalized AUC values for all identified metabolites representing the same molecular family based upon MS/MS fragmentation patterns were summed to provide the total AUC for the PCH or PVD molecular families.

ICP-MS analysis of PGM: Metals were quantified from 2.5% (w/v) PGM suspended in 1X MOPS using inductively coupled plasma mass spectrometry (ICP-MS) analysis at the University of Nebraska - Lincoln Spectroscopy and Biophysics Core facility. Samples were diluted 1:1 with nitric acid, digested overnight, and diluted an additional 10-fold before analysis conducting ICP-MS (Agilent 7500 cx). Gallium (Ga), 50 ppb, was added to each sample as an internal standard. Samples were analyzed in technical triplicate with a blank wash run between each sample. Only concentrations above the limit of quantification were retained. To determine the amount of iron added to media by

the addition of PGM, or 1X MOPS when used in place of PGM (**Fig. 7 PGM iron content and impact on PAO1 siderophores**), the concentration of PGM was brought to that present in most ASM formulations (0.5% w/v) and converted to micromolar concentration.

Statistical analysis: Statistical comparison of FBMN features of *P. aeruginosa* cultured in ASM formulations was conducted on the sum normalized feature table (**Dataset S2 ASM statistical analysis**) using ANOVA with Tukey's correction for multiple comparisons in MetaboAnalyst 4.0 (108-111) (**Dataset S2 ASM statistical analyses**). Statistical comparison of individual metabolites, sub-structure classes, and molecular families performed using ANOVA with Tukey's multiple comparisons correction in GraphPad Prism (version 8.4.0) (**Dataset S2 ASM statistical analyses**). Statistical comparison of PCH and PVD production by *P. aeruginosa* in SCFM1 and SCFM1+PGM was conducted using a two tailed, unpaired t-test with Welch's correction for unequal standard deviations in GraphPad Prism (version 8.4.3). For all analyses, *P* values less than 0.05 were considered statistically significant.

Data availability: All mass spectrometry data including the raw files, .mzXML files, metadata table, and Cytoscape files are available via MassIVE (accession numbers: MSV000086721 (LB and ASM formulations – media control, *P. aeruginosa* culture, QC, and PA mix data) and MSV000086723 (SCFM1 and PGM-SCFM1 – media control, *P. aeruginosa* culture, QC, and PA mix data)).

ACKNOWLEDGEMENTS:

We are very grateful to Mingxun Wang (University of California, San Diego) for providing input and beta versions of the networking software for metabolomics analysis;

Laura Sanchez, Jacob Porter, and Katherine Zink (University of Illinois, Chicago) for providing initial collection of metabolomics data; and members of the Phelan lab for thoughtful discussion about and suggestions on improving this manuscript.

REFERENCES

1. Sanders NN, Van Rompaey E, De Smedt SC, Demeester J. 2001. Structural Alterations of Gene Complexes by Cystic Fibrosis Sputum. American Journal of Respiratory and Critical Care Medicine 164:486-493.
2. Schwab U, Abdullah LH, Perlmutt OS, Albert D, Davis CW, Arnold RR, Yankaskas JR, Gilligan P, Neubauer H, Randell SH, Boucher RC. 2014. Localization of Burkholderia cepacia complex bacteria in cystic fibrosis lungs and interactions with Pseudomonas aeruginosa in hypoxic mucus. Infection and Immunity 82:4729-4745.
3. Fung C, Naughton S, Turnbull L, Tingpej P, Rose B, Arthur J, Hu HH, Harmer C, Harbour C, Hassett DJ, Whitchurch CB, Manos J. 2010. Gene expression of Pseudomonas aeruginosa in a mucin-containing synthetic growth medium mimicking cystic fibrosis lung sputum. Journal of Medical Microbiology 59:1089-1100.
4. Ghani M, Soothill JS. 1997. Ceftazidime, gentamicin, and rifampicin, in combination, kill biofilms of mucoid Pseudomonas aeruginosa. Canadian Journal of Microbiology 43:999-1004.
5. Hare NJ, Soe CZ, Rose B, Harbour C, Codd R, Manos J, Cordwell SJ. 2012. Proteomics of Pseudomonas aeruginosa Australian Epidemic Strain 1 (AES-1)

Cultured under Conditions Mimicking the Cystic Fibrosis Lung Reveals Increased Iron Acquisition via the Siderophore Pyochelin. Journal of Proteome Research 11:776-795.

6. Kirchner S, Fothergill JL, Wright EA, James CE, Mowat E, Winstanley C. 2012. Use of Artificial Sputum Medium to Test Antibiotic Efficacy Against Pseudomonas aeruginosa in Conditions More Relevant to the Cystic Fibrosis Lung. Jove-Journal of Visualized Experiments doi:ARTN e3857 10.3791/3857.

7. Palmer KL, Aye LA, Whiteley M. 2007. Nutritional cues control Pseudomonas aeruginosa multicellular Behavior in cystic fibrosis sputum. Journal of Bacteriology 189:8079-8087.

8. Quinn RA, Whiteson K, Lim YW, Salamon P, Bailey B, Mienardi S, Sanchez SE, Blake D, Conrad D, Rohwer F. 2015. A Winogradsky-based culture system shows an association between microbial fermentation and cystic fibrosis exacerbation (vol 9, pg 1024, 2015). Isme Journal 9:1052-1052.

9. Sriramulu DD. 2010. Artifical Sputum Medium. Protocol Exchange doi:doi:10.1038/protex.2010.212.

10. Sriramulu DD, Lunsdorf H, Lam JS, Romling U. 2005. Microcolony formation: a novel biofilm model of Pseudomonas aeruginosa for the cystic fibrosis lung. Journal of Medical Microbiology 54:667-676.

11. Turner KH, Wessel AK, Palmer GC, Murray JL, Whiteley M. 2015. Essential genome of Pseudomonas aeruginosa in cystic fibrosis sputum. Proceedings of the National Academy of Sciences of the United States of America 112:4110-4115.

12. Homa M, Sandor A, Toth E, Szebenyi C, Nagy G, Vagvolgyi C, Papp T. 2019. In vitro Interactions of Pseudomonas aeruginosa With Scedosporium Species Frequently Associated With Cystic Fibrosis. Front Microbiol 10:441.

13. Schick A, Kassen R. 2018. Rapid diversification of Pseudomonas aeruginosa in cystic fibrosis lung-like conditions. Proc Natl Acad Sci U S A 115:10714-10719.

14. Wong A, Rodrigue N, Kassen R. 2012. Genomics of adaptation during experimental evolution of the opportunistic pathogen Pseudomonas aeruginosa. PLoS Genet 8:e1002928.

15. Behrends V, Geier B, Williams HD, Bundy JG. 2013. Direct Assessment of Metabolite Utilization by Pseudomonas aeruginosa during Growth on Artificial Sputum Medium. Applied and Environmental Microbiology 79:2467-2470.

16. Darch SE, Simoska O, Fitzpatrick M, Barraza JP, Stevenson KJ, Bonnecaze RT, Shear JB, Whiteley M. 2018. Spatial determinants of quorum signaling in a Pseudomonas aeruginosa infection model. Proceedings of the National Academy of Sciences 115:4779-4784.

17. Behrends V, Ebbels TMD, Williams HD, Bundy JG. 2009. Time-Resolved Metabolic Footprinting for Nonlinear Modeling of Bacterial Substrate Utilization. Applied and Environmental Microbiology 75:2453-2463.

18. Haley CL, Colmer-Hamood JA, Hamood AN. 2012. Characterization of biofilm-like structures formed by Pseudomonas aeruginosa in a synthetic mucus medium. BMC Microbiology 12:181.

19. Diaz Iglesias Y, Van Bambeke F. 2020. Activity of Antibiotics against Pseudomonas aeruginosa in an In Vitro Model of Biofilms in the Context of Cystic Fibrosis: Influence of the Culture Medium. Antimicrobial Agents and Chemotherapy 64.

20. Stevens DA, Moss RB, Hernandez C, Clemons KV, Martinez M. 2016. Effect of Media Modified To Mimic Cystic Fibrosis Sputum on the Susceptibility of Aspergillus fumigatus, and the Frequency of Resistance at One Center. Antimicrob Agents Chemother 60:2180-4.

21. Lightly TJ, Phung RR, Sorensen JL, Cardona ST. 2017. Synthetic cystic fibrosis sputum medium diminishes Burkholderia cenocepacia antifungal activity against Aspergillus fumigatus independently of phenylacetic acid production. Canadian Journal of Microbiology 63:427-438.

22. Kirchhoff L, Weisner A-K, Schrepffer M, Hain A, Scharmann U, Buer J, Rath P-M, Steinmann J. 2020. Phenotypical Characteristics of the Black Yeast Exophiala dermatitidis Are Affected by Pseudomonas aeruginosa in an Artificial Sputum Medium Mimicking Cystic Fibrosis–Like Conditions. Frontiers in Microbiology 11.

23. Limoli DH, Whitfield GB, Kitao T, Ivey ML, Davis MR, Grahl N, Hogan DA, Rahme LG, Howell PL, O'Toole GA, Goldberg JB. 2017. Pseudomonas aeruginosa Alginate Overproduction Promotes Coexistence with Staphylococcus aureus in a Model of Cystic Fibrosis Respiratory Infection. mBio 8.

24. Colmer-Hamood JA, Dzvova N, Kruczek C, Hamood AN. 2016. In Vitro Analysis of Pseudomonas aeruginosa Virulence Using Conditions That Mimic the Environment at Specific Infection Sites, p 151-191, Progress in Molecular Biology and Translational Science, vol 142. Elsevier.

25. Foundation CF. 2019. 2018 Annual Data Report. Bethesda, Maryland.

26. Konstan MW, Wagener JS, VanDevanter DR, Pasta DJ, Yegin A, Rasouliyan L, Morgan WJ. 2012. Risk factors for rate of decline in FEV1 in adults with cystic fibrosis. Journal of Cystic Fibrosis 11:405-411.

27. Bianconi I, Jeukens J, Freschi L, Alcalá-Franco B, Facchini M, Boyle B, Molinaro A, Kukavica-Ibrulj I, Tümmler B, Levesque RC, Bragonzi A. 2015. Comparative

genomics and biological characterization of sequential Pseudomonas aeruginosa isolates from persistent airways infection. BMC Genomics 16.

28. Ciofu O, Tolker-Nielsen T, Jensen PØ, Wang H, Høiby N. 2015. Antimicrobial resistance, respiratory tract infections and role of biofilms in lung infections in cystic fibrosis patients. Advanced Drug Delivery Reviews 85:7-23.

29. Winstanley C, O'Brien S, Brockhurst MA. 2016. Pseudomonas aeruginosa Evolutionary Adaptation and Diversification in Cystic Fibrosis Chronic Lung Infections. Trends in Microbiology 24:327-337.

30. Feliziani S, Luján AM, Moyano AJ, Sola C, Bocco JL, Montanaro P, Canigia LF, Argaraña CE, Smania AM. 2010. Mucoidy, Quorum Sensing, Mismatch Repair and Antibiotic Resistance in Pseudomonas aeruginosa from Cystic Fibrosis Chronic Airways Infections. PLoS ONE 5:e12669.

31. Mouton JW, den Hollander JG, Horrevorts AM. 1993. Emergence of antibiotic resistance amongst Pseudomonas aeruginosa isolates from patients with cystic fibrosis. Journal of Antimicrobial Chemotherapy 31:919-926.

32. Martin LW, Reid DW, Sharples KJ, Lamont IL. 2011. <Emphasis Type="Italic">Pseudomonas</Emphasis> siderophores in the sputum of patients with cystic fibrosis. BioMetals 24:1059-1067.

33. Quinn RA, Phelan VV, Whiteson KL, Garg N, Bailey BA, Lim YW, Conrad DJ, Dorrestein PC, Rohwer FL. 2016. Microbial, host and xenobiotic diversity in the cystic fibrosis sputum metabolome. The ISME Journal 10:1483-1498.

34. Workentine ML, Sibley CD, Glezerson B, Purighalla S, Norgaard-Gron JC, Parkins MD, Rabin HR, Surette MG. 2013. Phenotypic Heterogeneity of Pseudomonas aeruginosa Populations in a Cystic Fibrosis Patient. PLoS ONE 8:e60225.

35. Diggle SP, Matthijs S, Wright VJ, Fletcher MP, Chhabra SR, Lamont IL, Kong X, Hider RC, Cornelis P, Cámara M, Williams P. 2007. The Pseudomonas aeruginosa 4-Quinolone Signal Molecules HHQ and PQS Play Multifunctional Roles in Quorum Sensing and Iron Entrapment. Chemistry & Biology 14:87-96.

36. Wang Y, Kern SE, Newman DK. 2010. Endogenous Phenazine Antibiotics Promote Anaerobic Survival of Pseudomonas aeruginosa via Extracellular Electron Transfer. Journal of Bacteriology 192:365-369.

37. Caiazza NC, Shanks RMQ, O'Toole GA. 2005. Rhamnolipids Modulate Swarming Motility Patterns of Pseudomonas aeruginosa. Journal of Bacteriology 187:7351-7361.

38. Cornelis P. 2010. Iron uptake and metabolism in pseudomonads. Applied Microbiology and Biotechnology 86:1637-1645.

39. Cox CD, Adams P. 1985. Siderophore activity of pyoverdin for Pseudomonas aeruginosa. Infection and Immunity 48:130-138.

40. Briard B, Bomme P, Lechner BE, Mislin GLA, Lair V, Prévost M-C, Latgé J-P, Haas H, Beauvais A. 2015. Pseudomonas aeruginosa manipulates redox and iron homeostasis of its microbiota partner Aspergillus fumigatus via phenazines. Scientific Reports 5.

41. Briard B, Rasoldier V, Bomme P, ElAouad N, Guerreiro C, Chassagne P, Muszkieta L, Latgé J-P, Mulard L, Beauvais A. 2017. Dirhamnolipids secreted from Pseudomonas aeruginosa modify anjpegungal susceptibility of Aspergillus fumigatus by inhibiting β1,3 glucan synthase activity. The ISME Journal 11:1578-1591.

42. Costello A, Reen FJ, O'Gara F, Callaghan M, McClean S. 2014. Inhibition of co-colonizing cystic fibrosis-associated pathogens by Pseudomonas aeruginosa and Burkholderia multivorans. Microbiology (Reading, England) 160:1474-1487.

43. Wang M, Carver JJ, Phelan VV, Sanchez LM, Garg N, Peng Y, Nguyen DD, Watrous J, Kapono CA, Luzzatto-Knaan T, Porto C, Bouslimani A, Melnik AV, Meehan MJ, Liu W-T, Crüsemann M, Boudreau PD, Esquenazi E, Sandoval-Calderón M, Kersten RD, Pace LA, Quinn RA, Duncan KR, Hsu C-C, Floros DJ, Gavilan RG, Kleigrewe K, Northen T, Dutton RJ, Parrot D, Carlson EE, Aigle B,

Michelsen CF, Jelsbak L, Sohlenkamp C, Pevzner P, Edlund A, McLean J, Piel J, Murphy BT, Gerwick L, Liaw C-C, Yang Y-L, Humpf H-U, Maansson M, Keyzers RA, Sims AC, Johnson AR, Sidebottom AM, Sedio BE, et al. 2016. Sharing and community curation of mass spectrometry data with Global Natural Products Social Molecular Networking. Nature Biotechnology 34:828-837.

44. Nothias LF, Petras D, Schmid R, Duhrkop K, Rainer J, Sarvepalli A, Protsyuk I, Ernst M, Tsugawa H, Fleischauer M, Aicheler F, Aksenov AA, Alka O, Allard PM, Barsch A, Cachet X, Caraballo-Rodriguez AM, Da Silva RR, Dang T, Garg N, Gauglitz JM, Gurevich A, Isaac G, Jarmusch AK, Kamenik Z, Kang KB, Kessler N, Koester I, Korf A, Le Gouellec A, Ludwig M, Martin HC, McCall LI, McSayles J, Meyer SW, Mohimani H, Morsy M, Moyne O, Neumann S, Neuweger H, Nguyen NH, Nothias-Esposito M, Paolini J, Phelan VV, Pluskal T, Quinn RA, Rogers S, Shrestha B, Tripathi A, van der Hooft JJJ, et al. 2020. Feature-based molecular networking in the GNPS analysis environment. Nat Methods doi:10.1038/s41592-020-0933-6.

45. La Rosa R, Johansen HK, Molin S. 2019. Adapting to the Airways: Metabolic Requirements of Pseudomonas aeruginosa during the Infection of Cystic Fibrosis Patients. Metabolites 9.

46. Phelan VV, Liu WT, Pogliano K, Dorrestein PC. 2011. Microbial metabolic exchange--the chemotype-to-phenotype link. Nat Chem Biol 8:26-35.

47. Schmidt R, Ulanova D, Wick LY, Bode HB, Garbeva P. 2019. Microbe-driven chemical ecology: past, present and future. ISME J 13:2656-2663.

48. Phelan VV, Moree WJ, Aguilar J, Cornett DS, Koumoutsi A, Noble SM, Pogliano K, Guerrero CA, Dorrestein PC. 2014. Impact of a Transposon Insertion in phzF2 on the Specialized Metabolite Production and Interkingdom Interactions of Pseudomonas aeruginosa. Journal of Bacteriology 196:1683-1693.

49. Phelan VV, Fang J, Dorrestein PC. 2015. Mass Spectrometry Analysis of Pseudomonas aeruginosa Treated with Azithromycin. J Am Soc Mass Spectrom 26:873-7.

50. Condren AR, Kahl LJ, Boelter G, Kritikos G, Banzhaf M, Dietrich LEP, Sanchez LM. 2020. Biofilm Inhibitor Taurolithocholic Acid Alters Colony Morphology, Specialized Metabolism, and Virulence of Pseudomonas aeruginosa. ACS Infect Dis 6:603-612.

51. Depke T, Thöming JG, Kordes A, Häussler S, Brönstrup M. 2020. Untargeted LC-MS Metabolomics Differentiates Between Virulent and Avirulent Clinical Strains of Pseudomonas aeruginosa. Biomolecules 10:1041.

52. Purves K, Macintyre L, Brennan D, Hreggviðsson G, Kuttner E, Ásgeirsdóttir M, Young L, Green D, Edrada-Ebel R, Duncan K. 2016. Using Molecular Networking for Microbial Secondary Metabolite Bioprospecting. Metabolites 6:2.

53. Caraballo-Rodríguez AM, Dorrestein PC, Pupo MT. 2017. Molecular inter-kingdom interactions of endophytes isolated from Lychnophora ericoides. Scientific Reports 7.

54. Das T, Manefield M. 2012. Pyocyanin Promotes Extracellular DNA Release in Pseudomonas aeruginosa. PLoS ONE 7:e46718.

55. Das T, Manefield M. 2013. Phenazine production enhances extracellular DNA release via hydrogen peroxide generation in Pseudomonas aeruginosa. Communicative & Integrative Biology 6:e23570.

56. Moree WJ, Phelan VV, Wu CH, Bandeira N, Cornett DS, Duggan BM, Dorrestein PC. 2012. Interkingdom metabolic transformations captured by microbial imaging mass spectrometry. Proceedings of the National Academy of Sciences of the United States of America 109:13811-13816.

57. Noto MJ, Burns WJ, Beavers WN, Skaar EP. 2017. Mechanisms of Pyocyanin Toxicity and Genetic Determinants of Resistance in Staphylococcus aureus. Journal of Bacteriology 199.

58. Das T, Kutty SK, Tavallaie R, Ibugo AI, Panchompoo J, Sehar S, Aldous L, Yeung AWS, Thomas SR, Kumar N, Gooding JJ, Manefield M. 2015. Phenazine virulence factor binding to extracellular DNA is important for Pseudomonas aeruginosa biofilm formation. Scientific Reports 5.

59. Wilson R, Pitt T, Taylor G, Watson D, MacDermot J, Sykes D, Roberts D, Cole P. 1987. Pyocyanin and 1-hydroxyphenazine produced by Pseudomonas aeruginosa inhibit the beating of human respiratory cilia in vitro. Journal of Clinical Investigation 79:221-229.

60. Allen L, Dockrell DH, Pattery T, Lee DG, Cornelis P, Hellewell PG, Whyte MKB. 2005. Pyocyanin Production by Pseudomonas aeruginosa Induces Neutrophil Apoptosis and Impairs Neutrophil-Mediated Host Defenses In Vivo. The Journal of Immunology 174:3643-3649.

61. Wang Y, Wilks JC, Danhorn T, Ramos I, Croal L, Newman DK. 2011. Phenazine-1-Carboxylic Acid Promotes Bacterial Biofilm Development via Ferrous Iron Acquisition. Journal of Bacteriology 193:3606-3617.

62. Schalk IJ, Guillon L. 2013. Pyoverdine biosynthesis and secretion in Pseudomonas aeruginosa : implications for metal homeostasis: Pyoverdine biosynthesis. Environmental Microbiology 15:1661-1673.

63. Gasser V, Guillon L, Cunrath O, Schalk IJ. 2015. Cellular organization of siderophore biosynthesis in Pseudomonas aeruginosa: Evidence for siderosomes. Journal of Inorganic Biochemistry 148:27-34.

64. Cox CD, Rinehart KL, Moore ML, Cook JC. 1981. Pyochelin: novel structure of an iron-chelating growth promoter for Pseudomonas aeruginosa. Proceedings of the National Academy of Sciences 78:4256-4260.

65. Korgaonkar AK, Whiteley M. 2011. Pseudomonas aeruginosa enhances production of an antimicrobial in response to N-acetylglucosamine and peptidoglycan. J Bacteriol 193:909-17.

66. Van Ark G, Berden JA. 1977. Binding of HQNO to beef-heart sub-mitochondrial particles. Biochimica et Biophysica Acta (BBA) - Bioenergetics 459:119-137.

67. Hazan R, Que Yok A, Maura D, Strobel B, Majcherczyk Paul A, Hopper Laura R, Wilbur David J, Hreha Teri N, Barquera B, Rahme Laurence G. 2016. Auto Poisoning of the Respiratory Chain by a Quorum-Sensing-Regulated Molecule Favors Biofilm Formation and Antibiotic Tolerance. Current Biology 26:195-206.

68. Rampioni G, Falcone M, Heeb S, Frangipani E, Fletcher MP, Dubern J-F, Visca P, Leoni L, Cámara M, Williams P. 2016. Unravelling the Genome-Wide Contributions of Specific 2-Alkyl-4-Quinolones and PqsE to Quorum Sensing in Pseudomonas aeruginosa. PLOS Pathogens 12:e1006029.

69. McKnight SL, Iglewski BH, Pesci EC. 2000. The Pseudomonas Quinolone Signal Regulates rhl Quorum Sensing in Pseudomonas aeruginosa. Journal of Bacteriology 182:2702-2708.

70. Guo Q, Kong W, Jin S, Chen L, Xu Y, Duan K. 2014. PqsR-dependent and PqsR-independent regulation of motility and biofilm formation by PQS in Pseudomonas aeruginosa PAO1: Regulation of motility and biofilm by PQS. Journal of Basic Microbiology 54:633-643.

71. Lépine F, Milot S, Déziel E, He J, Rahme LG. 2004. Electrospray/mass spectrometric identification and analysis of 4-hydroxy-2-alkylquinolines (HAQs) produced by Pseudomonas aeruginosa. Journal of the American Society for Mass Spectrometry 15:862-869.

72. Davey ME, Caiazza NC, O'Toole GA. 2003. Rhamnolipid Surfactant Production Affects Biofilm Architecture in Pseudomonas aeruginosa PAO1. Journal of Bacteriology 185:1027-1036.

73. Glick R, Gilmour C, Tremblay J, Satanower S, Avidan O, Déziel E, Greenberg EP, Poole K, Banin E. 2010. Increase in Rhamnolipid Synthesis under Iron-Limiting Conditions Influences Surface Motility and Biofilm Formation in Pseudomonas aeruginosa. Journal of Bacteriology 192:2973-2980.

74. McClure CD, Schiller NL. 1996. Inhibition of Macrophage Phagocytosis by Pseudomonas aeruginosa Rhamnolipids In Vitro and In Vivo. Current Microbiology 33:109-117.

75. Zulianello L, Canard C, Köhler T, Caille D, Lacroix J-S, Meda P. 2006. Rhamnolipids Are Virulence Factors That Promote Early Infiltration of Primary Human Airway Epithelia by Pseudomonas aeruginosa. Infection and Immunity 74:3134-3147.

76. Ochsner UA, Reiser J. 1995. Autoinducer-mediated regulation of rhamnolipid biosurfactant synthesis in Pseudomonas aeruginosa. Proceedings of the National Academy of Sciences 92:6424-6428.

77. Schuster M, Greenberg EP. 2007. Early activation of quorum sensing in Pseudomonas aeruginosa reveals the architecture of a complex regulon. BMC Genomics 8:287.

78. Whiteley M, Lee KM, Greenberg EP. 1999. Identification of genes controlled by quorum sensing in Pseudomonas aeruginosa. Proceedings of the National Academy of Sciences 96:13904-13909.

79. Meyer JM, Neely A, Stintzi A, Georges C, Holder IA. 1996. Pyoverdin is essential for virulence of Pseudomonas aeruginosa. Infection and Immunity 64:518-523.

80. Takase H, Nitanai H, Hoshino K, Otani T. 2000. Impact of Siderophore Production onPseudomonas aeruginosa Infections in Immunosuppressed Mice. Infection and Immunity 68:1834-1839.

81. Sriyosachati S, Cox CD. 1986. Siderophore-mediated iron acquisition from transferrin by Pseudomonas aeruginosa. Infection and Immunity 52:885-891.

82. Ochsner UA, Vasil AI, Vasil ML. 1995. Role of the ferric uptake regulator of Pseudomonas aeruginosa in the regulation of siderophores and exotoxin A expression: purification and activity on iron-regulated promoters. Journal of bacteriology 177:7194-7201.

83. Co JY, Cárcamo-Oyarce G, Billings N, Wheeler KM, Grindy SC, Holten-Andersen N, Ribbeck K. 2018. Mucins trigger dispersal of Pseudomonas aeruginosa biofilms. npj Biofilms and Microbiomes 4.

84. Wheeler KM, Cárcamo-Oyarce G, Turner BS, Dellos-Nolan S, Co JY, Lehoux S, Cummings RD, Wozniak DJ, Ribbeck K. 2019. Mucin glycans attenuate the virulence of Pseudomonas aeruginosa in infection. Nature Microbiology 4:2146-2154.

85. Paone P, Cani PD. 2020. Mucus barrier, mucins and gut microbiota: the expected slimy partners? Gut 69:2232-2243.

86. Wagner CE, Wheeler KM, Ribbeck K. 2018. Mucins and Their Role in Shaping the Functions of Mucus Barriers. Annual Review of Cell and Developmental Biology 34:189-215.

87. Hoffman CL, Lalsiamthara J, Aballay A. 2020. Host Mucin Is Exploited by Pseudomonas aeruginosa To Provide Monosaccharides Required for a Successful Infection. mBio 11.

88. Flynn JM, Niccum D, Dunitz JM, Hunter RC. 2016. Evidence and Role for Bacterial Mucin Degradation in Cystic Fibrosis Airway Disease. PLOS Pathogens 12:e1005846.

89. Darch SE, Kragh KN, Abbott EA, Bjarnsholt T, Bull JJ, Whiteley M. 2017. Phage Inhibit Pathogen Dissemination by Targeting Bacterial Migrants in a Chronic Infection Model. mBio 8.

90. Secor PR, Michaels LA, Ratjen A, Jennings LK, Singh PK. 2018. Entropically driven aggregation of bacteria by host polymers promotes antibiotic tolerance in Pseudomonas aeruginosa. Proceedings of the National Academy of Sciences 115:10780-10785.

91. Hao Y, Kuang Z, Walling BE, Bhatia S, Sivaguru M, Chen Y, Gaskins HR, Lau GW. 2012. Pseudomonas aeruginosa pyocyanin causes airway goblet cell hyperplasia and metaplasia and mucus hypersecretion by inactivating the

transcriptional factor FoxA2: Pseudomonas pyocyanin inactivates airway FoxA2. Cellular Microbiology 14:401-415.

92. Kanthakumar K, Taylor G, Tsang KW, Cundell DR, Rutman A, Smith S, Jeffery PK, Cole PJ, Wilson R. 1993. Mechanisms of action of Pseudomonas aeruginosa pyocyanin on human ciliary beat in vitro. Infection and Immunity 61:2848-2853.

93. O'Malley YQ, Reszka KJ, Spitz DR, Denning GM, Britigan BE. 2004. Pseudomonas aeruginosa pyocyanin directly oxidizes glutathione and decreases its levels in airway epithelial cells. American Journal of Physiology-Lung Cellular and Molecular Physiology 287:L94-L103.

94. Schwarzer C, Fischer H, Kim E-J, Barber KJ, Mills AD, Kurth MJ, Gruenert DC, Suh JH, Machen TE, Illek B. 2008. Oxidative stress caused by pyocyanin impairs CFTR Cl− transport in human bronchial epithelial cells. Free Radical Biology and Medicine 45:1653-1662.

95. Moree WJ, Phelan VV, Wu C-H, Bandeira N, Cornett DS, Duggan BM, Dorrestein PC. 2012. Interkingdom metabolic transformations captured by microbial imaging mass spectrometry. Proceedings of the National Academy of Sciences 109:13811-13816.

96. Orazi G, Jean-Pierre F, O'Toole GA. 2020. Pseudomonas aeruginosa PA14 Enhances the Efficacy of Norfloxacin against Staphylococcus aureus Newman Biofilms. Journal of Bacteriology 202.

97. Minandri F, Imperi F, Frangipani E, Bonchi C, Visaggio D, Facchini M, Pasquali P, Bragonzi A, Visca P. 2016. Role of Iron Uptake Systems in Pseudomonas aeruginosa Virulence and Airway Infection. Infection and Immunity 84:2324-2335.

98. Kilbourn JP. 1984. Composition of sputum from patients with cystic fibrosis. Current Microbiology 11:19-22.

99. Hunter RC, Asfour F, Dingemans J, Osuna BL, Samad T, Malfroot A, Cornelis P, Newman DK. 2013. Ferrous Iron Is a Significant Component of Bioavailable Iron in Cystic Fibrosis Airways. mBio 4.

100. Reid DW, Carroll V, O'May C, Champion A, Kirov SM. 2007. Increased airway iron as a potential factor in the persistence of Pseudomonas aeruginosa infection in cystic fibrosis. European Respiratory Journal 30:286-292.

101. Ghio AJ, Roggli VL, Soukup JM, Richards JH, Randell SH, Muhlebach MS. 2013. Iron accumulates in the lavage and explanted lungs of cystic fibrosis patients. Journal of Cystic Fibrosis 12:390-398.

102. Jacobs MA, Alwood A, Thaipisuttikul I, Spencer D, Haugen E, Ernst S, Will O, Kaul R, Raymond C, Levy R, Chun-Rong L, Guenthner D, Bovee D, Olson MV, Manoil C. 2003. Comprehensive transposon mutant library of Pseudomonas aeruginosa. Proc Natl Acad Sci U S A 100:14339-44.

103. Shannon P, Markiel A, Ozier O, Baliga NS, Wang JT, Ramage D, Amin N, Schwikowski B, Ideker T. 2003. Cytoscape: A software environment for integrated models of biomolecular interaction networks. Genome Research 13:2498-2504.

104. Conway JR, Lex A, Gehlenborg N. 2017. UpSetR: an R package for the visualization of intersecting sets and their properties. Bioinformatics 33:2938-2940.

105. Lex A, Gehlenborg N, Strobelt H, Vuillemot R, Pfister H. 2014. UpSet: Visualization of Intersecting Sets. IEEE Trans Vis Comput Graph 20:1983-92.

106. Pluskal T, Castillo S, Villar-Briones A, Oresic M. 2010. MZmine 2: Modular framework for processing, visualizing, and analyzing mass spectrometry-based molecular profile data. Bmc Bioinformatics 11.

107. Sumner LW, Amberg A, Barrett D, Beale MH, Beger R, Daykin CA, Fan TWM, Fiehn O, Goodacre R, Griffin JL, Hankemeier T, Hardy N, Harnly J, Higashi R, Kopka J, Lane AN, Lindon JC, Marriott P, Nicholls AW, Reily MD, Thaden JJ,

Viant MR. 2007. Proposed minimum reporting standards for chemical analysis. Metabolomics 3:211-221.

108. Chong J, Soufan O, Li C, Caraus I, Li S, Bourque G, Wishart DS, Xia J. 2018. MetaboAnalyst 4.0: towards more transparent and integrative metabolomics analysis. Nucleic Acids Res 46:W486-W494.

109. Chong J, Xia J. 2018. MetaboAnalystR: an R package for flexible and reproducible analysis of metabolomics data. Bioinformatics 34:4313-4314.

110. Chong J, Yamamoto M, Xia J. 2019. MetaboAnalystR 2.0: From Raw Spectra to Biological Insights. Metabolites 9.

111. Pang Z, Chong J, Li S, Xia J. 2020. MetaboAnalystR 3.0: Toward an Optimized Workflow for Global Metabolomics. Metabolites 10:186.

FIGURES

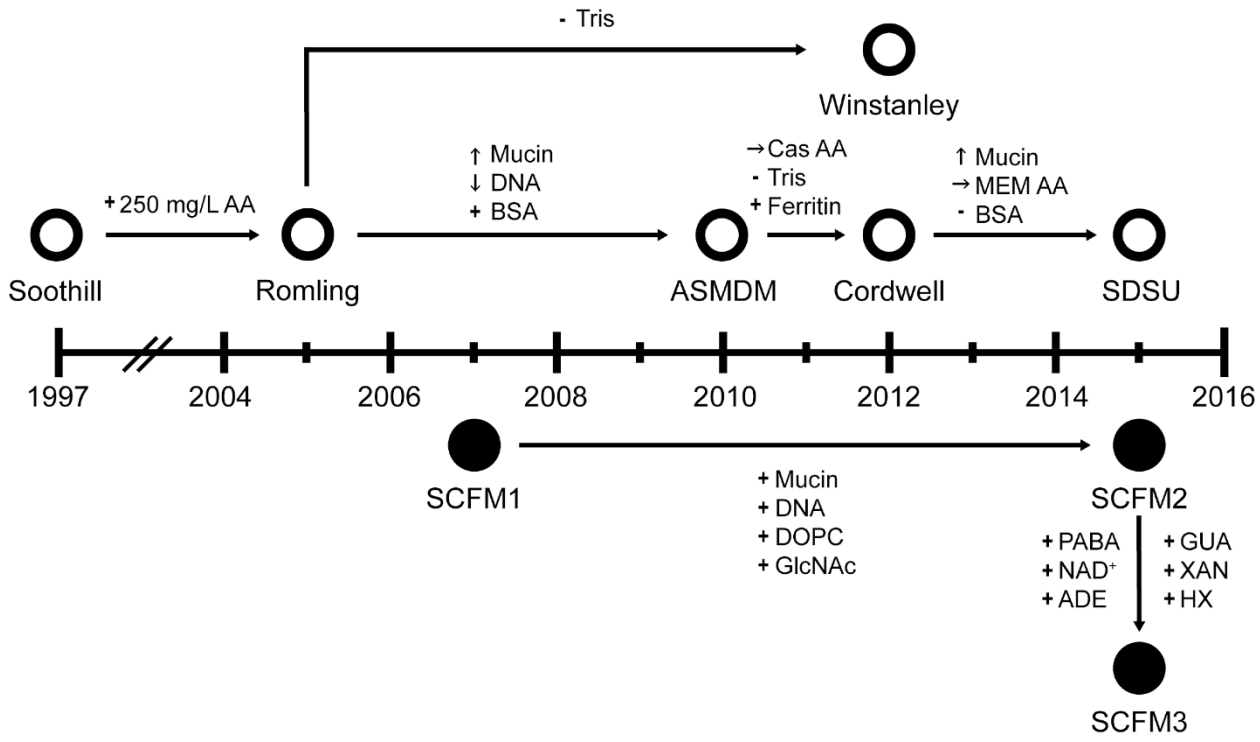

Figure 1 Timeline of ASM formulations. ASM formulations can be categorized into complex (open circles) or defined (closed circles) media. Each formulation is plotted at the year it was first published. Nutrient alterations between formulations are indicated by arrows. Compared to preceding formulation: + = added, - = removed, ↑ = increased, ↓ = decreased, → = different source. AA = amino acids, BSA = bovine serum albumin, Cas AA = casamino acids, MEM AA = MEM amino acids, DOPC = 1,2-dioleoyl-sn-glycero-3-phosphocholine, GlcNAc = *N*-acetylglucosamine, PABA = 4-aminobenzoic acid, NAD^+ = nicotinamide adenine dinucleotide, ADE = adenine, GUA = guanine, XAN = xanthine, HX = hypoxanthine. Recipes for ASM formulations are in detailed in *Dataset S1 ASM formulations*.

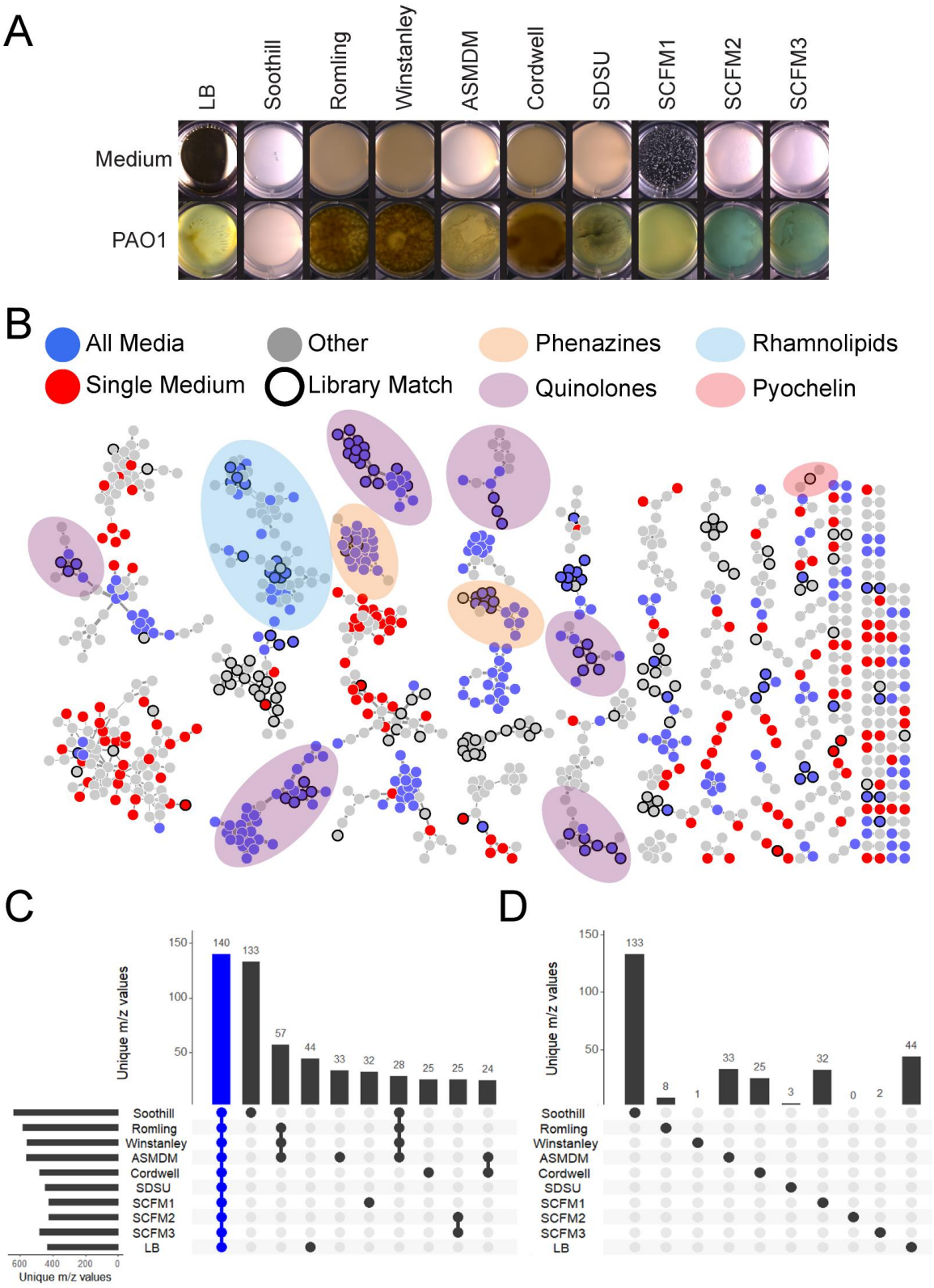
A
LB
Soothill
Romling
Winstanley
ASMDM
Cordwell
SDSU
SCFM1
SCFM2
SCFM3
Medium
PAO1
B
All Media
Single Medium
Other
Library Match
Phenazines
Quinolones
Rhamnolipids
Pyochelin
C
Unique m/z values
140
133
57
44
33
32
28
25
25
24
Soothill
Romling
Winstanley
ASMDM
Cordwell
SDSU
SCFM1
SCFM2
SCFM3
LB
600
400
200
0
Unique m/z values
D
Unique m/z values
133
8
1
33
25
3
32
0
2
44
Soothill
Romling
Winstanley
ASMDM
Cordwell
SDSU
SCFM1
SCFM2
SCFM3
LB

940

Figure 2 PAO1 phenotype and metabolome in ASM and LB. (A) Representative phenotypic images of *P. aeruginosa* PAO1 grown in ASM. LB was used as a positive control. **(B)** Classical molecular network of the exometabolome of *P. aeruginosa* PAO1 grown in ASM. LB was used as a positive control. Nodes representing MS/MS detected in all media are blue. Nodes representing MS/MS detected in a single medium are red. The primary molecular families of *P. aeruginosa* are highlighted. Nodes not connected to any other node (singletons) were removed for clarity. The full network can be accessed via the link in 'Materials and Methods'. **(C & D)** Upset plots of number of unique *m/z* values detected in the 10 media arranged by decreasing frequency (C) and increasing degree (D). Intersections shown were limited to improve visualization. Upset plot data analysis is detailed in *Supplemental Dataset – Upset Plot Generation and Results.*

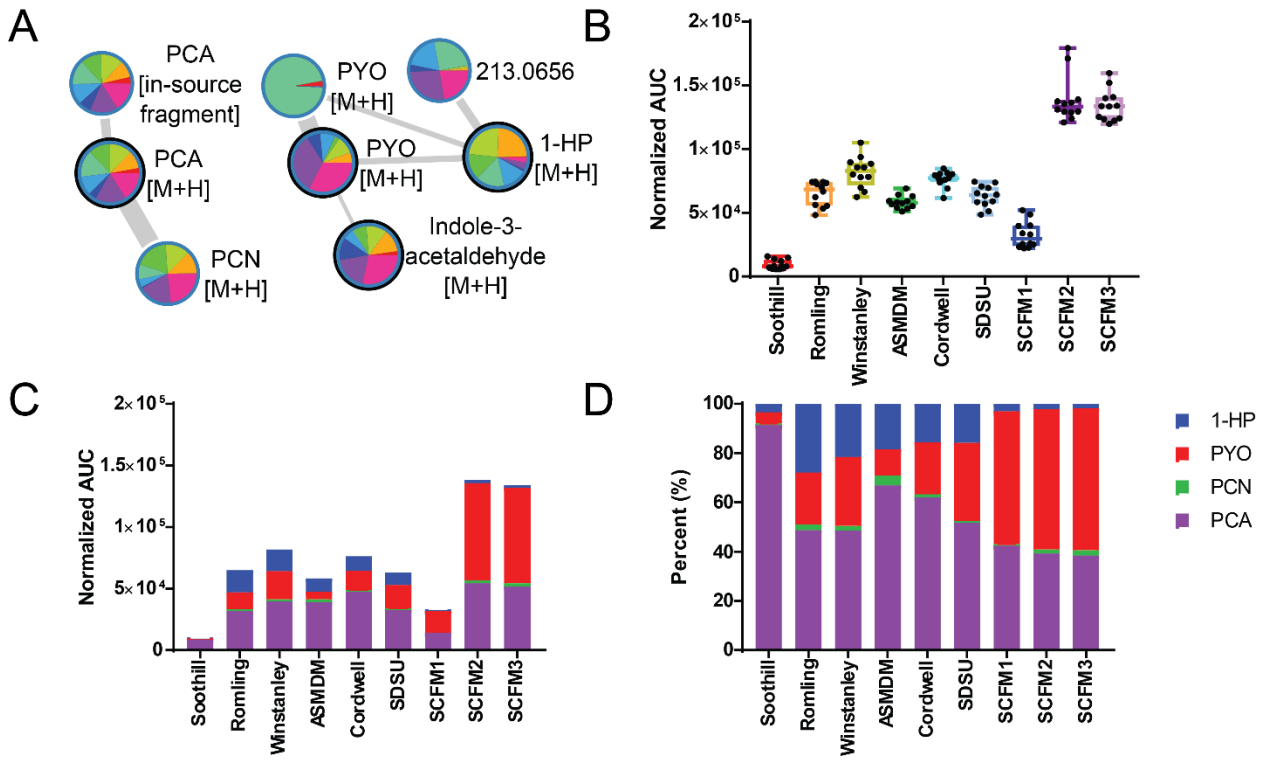

Figure 3 Phenazines Production in ASM. (A) Phenazine molecular family visualized with feature based molecular networking. Each node represents a feature, and relative abundance of each feature among ASM depicted by a pie chart. Pie charts are colored counterclockwise starting at three o'clock: Soothill red; Romling orange; Winstanley yellow; ASMDM green; Coldwell aqua; SDSU light blue; SCFM1 blue; SCFM2 purple; SCFM3 pink. GNPS library matches are indicated by black outlines. (B) Total normalized AUC for the phenazine molecular family in each ASM formulation depicted by box and whisker plot with individual samples shown (n=12 per ASM formulation). (C) Normalized AUC of each phenazine, stacked to show the phenazine profile of PAO1 in each ASM formulation. (D) Phenazine production in each ASM formulation as a percent of total phenazine production in the medium. (C, D) Phenazines from bottom to top of bars: PCA, phenazine-1-carboxylic acid, purple; PCN, phenazine-1-carboxamide, green; PYO, pyocyanin, red; 1-HP, 1-hydroxyphenazine, blue.

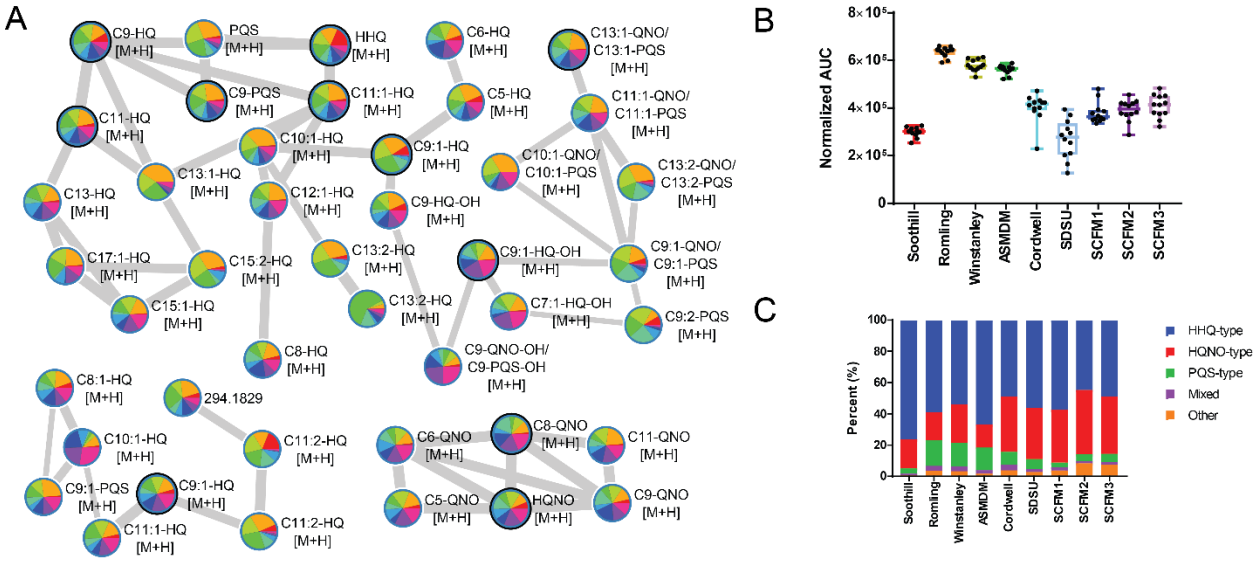

Figure 4 Quinolone Production in ASM. (A) Quinolone molecular family visualized with feature based molecular networking. Each node represents a feature, and relative abundance of each feature among ASM is depicted with a pie chart. Pie charts are colored counterclockwise starting at three o'clock: Soothill red; Romling orange; Winstanley yellow; ASMDM green; Cordwell aqua; SDSU light blue; SCFM1 blue; SCFM2 purple; SCFM3 pink. GNPS library matches are indicated by black outlines. (B) Total normalized AUC for the quinolone molecular family in each ASM formulation depicted by box and whisker plot with individual samples shown (n=12 per ASM formulation). (C) Quinolone subfamily production in each ASM formulation as a percent of total quinolone production in the medium. Quinolone subfamilies from top to bottom of bars: HHQ-type, blue; HQNO-type, red; PQS-type, green; Mixed, purple; Other, orange.

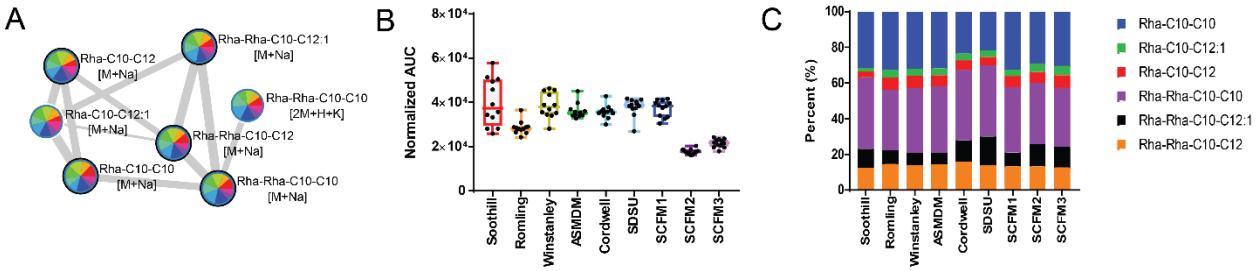

Figure 5 Rhamnolipid Production in ASM. (A) Rhamnolipid molecular family visualized with feature based molecular networking. Each node represents a feature, and relative abundance of each feature among ASM is depicted with a pie chart. Pie charts are colored counterclockwise starting at three o'clock: Soothill red; Romling orange; Winstanley yellow; ASMDM green; Cordwell aqua; SDSU light blue; SCFM1 blue; SCFM2 purple; SCFM3 pink. GNPS library matches are indicated by black

outlines. (B) Total normalized AUC for the rhamnolipid molecular family in each ASM formulation depicted by box and whisker plot with individual samples shown (n=12 per ASM formulation). (C) Rhamnolipid production in each ASM formulation as a percent of total rhamnolipid production in the medium. Rhamnolipids from top to bottom of bars: Rha-C10-C10, blue; Rha-C10-C12:1, green; Rha-C10-C12, red; Rha-Rha-C10-C10, purple; Rha-Rha-C10-C12:1, black; Rha-Rha-C10-C12, orange.

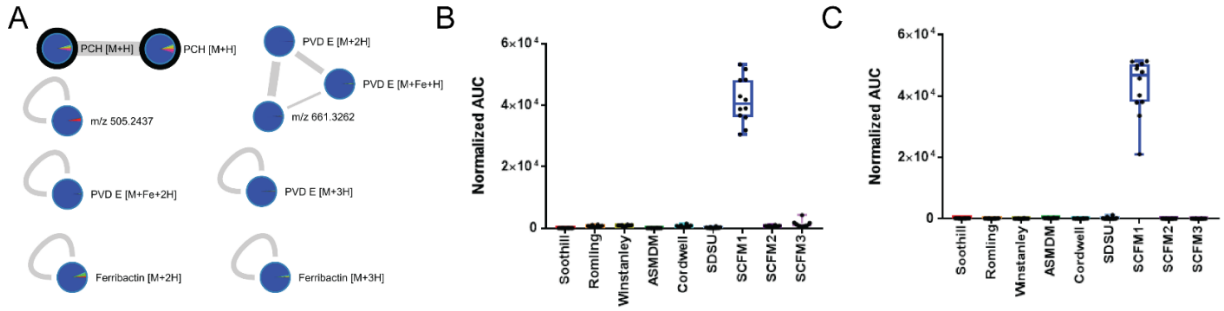

Figure 6 Siderophore Production in ASM. (A) PCH and PVD siderophore molecular families visualized with feature based molecular networking. Each node represents a feature, and relative abundance of each feature among ASM is depicted with a pie chart. Pie charts are colored counterclockwise starting at three o'clock: Soothill red; Romling orange; Winstanley yellow; ASMDM green; Cordwell aqua; SDSU light blue; SCFM1 blue; SCFM2 purple; SCFM3 pink. (B) Total normalized AUC for the PCH molecular family in each ASM formulation depicted by box and whisker plot with individual samples shown (n=12 per ASM formulation). (C) Total normalized AUC for the PVD molecular family in each ASM formulation depicted by box and whisker plot with individual samples shown (n=12 per ASM formulation).

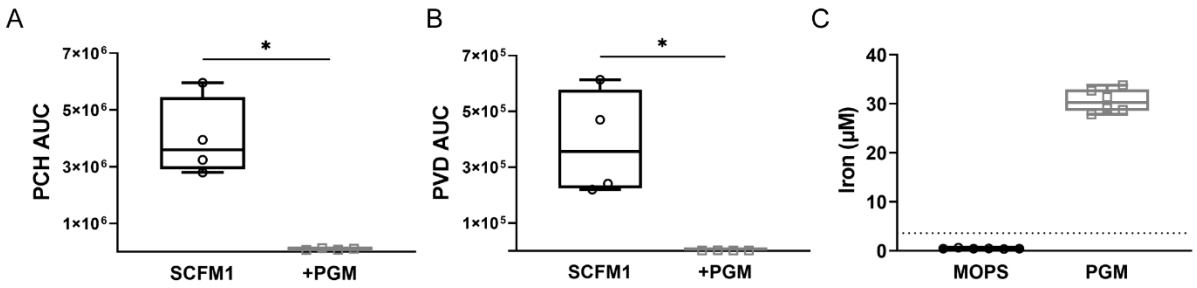

Figure 7 PGM iron content and impact on PAO1 siderophores. (A, B) Production of *P. aeruginosa* siderophores (A) pyochelin (PCH) and (B) pyoverdine (PVD) after growth in SCFM1 (black circles) and SCFM1 with mucin (+PGM, porcine gastric mucin; gray squares). The area under the curve (AUC) of four biological replicates are designated by box and whisker plots. Sample groups were compared using a two tailed, unpaired t test with Welch's correction, (A) *, p=0.0114; (B) *, p=0.0269. **(C)** Iron (^{56}Fe) was quantified from 1X MOPS and PGM by ICP-MS and the amount of iron added to SCFM1 by each component was determined. The iron concentration (μM) of six technical replicates are designated by box and whisker plots. The iron concentration added to SCFM1 (3.6 μM) is designated by the dotted line.

Supplemental Material

Figure S1 Growth of PAO1 in ASM. PAO1 was grown in nine ASM formulations and LB. Samples were prepared in three batches with LB growth included in each batch as a positive control. (A) Enumeration PAO1 of CFUs after growth in ASM formulations and LB. The means, standard error of the mean, and values of three biological replicates are shown. (B) Measurement of pH of PAO1 samples after growth in ASM formulations and LB. The mean and standard error of the mean and values of three biological replicates (open circles) are shown. The pH of each medium at inoculation is represented by a filled triangle.

Figure S2 Growth of PAO1 in SCFM1 with and without PGM. (A) Enumeration PAO1 of CFUs after growth in each SCFM1 and SCFM1 with PGM. The means, standard error of the mean, and values of four biological replicates are shown, $p<0.0001$ as determined by a two-tailed Student's *t* test. **(B)** Measurement of pH of PAO1 samples after growth in each SCFM1 and SCFM1 with PGM. The mean, standard error of the mean, and values of four biological replicates are shown, the dotted line represents the pH of the medium (pH = 7).

Figure S3 Pyovderdine chromatograms. Chromatogram traces of extracted ion chromatograms for the *m/z* values 667.3094 (PVD E [M+2H], blue); 693.7660 (PVD E [M+Fe+H], orange); 676.3333 (Ferribactin [M+2H], green); 505.2437 (red), and 661.3262 (purple) are shown with a tolerance of 20 ppm. Traces are all from a single representative SCFM1 sample from the dataset of PAO1 grown in ASM formulations visualized using the GNPS LCMS Dashboard (v0.25).

Table S1 ASM metabolite annotation and mass defect. Provides a table containing metabolite annotation, mass defect, and level of annotation from PAO1 cultures in ASM.

Table S2 SCFM1 and mucin siderophore annotation and mass defect. Provides a table containing metabolite annotation, mass defect, and level of annotation from PAO1 cultures in SCFM1 with and without mucin.